

## Longshore current forcing by irregular waves

B. D. Johnson and J. M. Smith

Coastal and Hydraulics Laboratory, Engineering Research and Development Center, Vicksburg, Mississippi, USA

Received 20 February 2004; revised 11 February 2005; accepted 11 March 2005; published 21 June 2005.

[1] The terms in the wave-averaged depth-integrated alongshore momentum balance are populated with detailed measurements from a laboratory basin experiment. Obliquely incident irregular waves were generated in a large wave basin equipped with instruments to collect free surface elevation and velocity measurements over a sand beach. Pumps matched the wave-generated currents, and experimental evidence indicates that the equations can justifiably be simplified by assuming alongshore uniformity. While the use of data measured below the trough level is straightforward, the velocity field in the region near the surface is extrapolated from the measured positions and constrained by conservation of cross-shore mass flux. The role of the dispersive mixing mechanism due to depth-dependent currents is shown to be small but acts to shift the peak of the longshore velocity shoreward slightly. Radiation stresses are the primary forcing mechanism, and computed stresses based on measured wave-induced hydrodynamics are considerably smaller than the widely used linear representation, indicating that the small-amplitude assumption of linear theory is not appropriate in the surf zone. The time-averaged bottom shear stress remains as the primary balance to the gradient in alongshore momentum, and the inferred shear stress compares favorably with the values computed using the quadratic drag law and a spatially constant friction coefficient.

**Citation:** Johnson, B. D., and J. M. Smith (2005), Longshore current forcing by irregular waves, *J. Geophys. Res.*, *110*, C06006, doi:10.1029/2004JC002336.

### 1. Introduction

[2] Nearshore hydrodynamics are responsible for the evolution of beach morphology, which is the focus of most coastal engineering projects. Typically the hydrodynamics are examined at two distinct timescales, with a time-averaging procedure that parameterizes the short-wave motions as a forcing function for the low-frequency or steady currents. The verification of this concept has generally been limited to field studies or laboratory tests in flumes. While field studies avoid the inevitable boundary effects encountered in the laboratory, these investigations suffer the complexities of bathymetric nonuniformities, wind stress, tidal fluctuations, longshore pressure gradients, and lack data collection density [e.g., Thornton and Guza, 1981; Feddersen *et al.*, 1998; Soulsby, 1998]. Flume studies, on the other hand, offer the opportunity to collect detailed hydrodynamic data in a controlled environment, but are restricted to colinear waves and wave-induced or pumped currents. Stive and Wind [1982], for instance, used detailed laboratory measurements to determine the cross-shore component of radiation stress. Rather than use velocity field measurements to develop expressions for  $S_{xx}$ , Svendsen and Putrevu [1993] used the measured slope of the mean free surface elevation while neglecting the small bottom shear stress to infer the gradients of the radiation stress. Using the slope of the free surface elevation is viable for the deter-

mination of  $S_{xx}$ ; in the case of the off diagonal component  $S_{xy}$ , however, no simple alternative exists to hydrodynamic measurements. Previous laboratory studies conducted in wave basins have utilized the linear representation of radiation stress [e.g., Visser, 1984], and others have included the effect of a roller [Reniers and Battjes, 1997].

[3] It is the intent of this present effort to provide insight into the longshore current forcing due to irregular waves over a movable bed through a careful treatment of the free surface elevation and velocity field data in a laboratory facility. This work begins with a concise description of the wave basin and the data collection suite. The irregular incident waves are described in terms of the measured values seaward of the breaking region. A method is presented that uses the internal velocity field to extrapolate into the upper region of the water column. The momentum fluxes are then determined, and the vertical variation is presented. The depth-integrated momentum flux is determined to be considerably smaller when compared to the widely used linear representation of the radiation stress. The momentum flux gradient is then shown to compare well with a simple bottom shear stress model. Finally, the cross-shore variation of the drag coefficient in the bottom stress model is determined by balancing the momentum equation.

### 2. Governing Equation

[4] While many problems must be treated in two horizontal dimensions, the laboratory design and measured data justify the assumption of alongshore uniformity in the



**Figure 1.** Movable bridge spanning the Large-Scale Sediment Transport Facility (LSTF).

presence of a longshore current. By collapsing this problem to one dimension, the alongshore momentum balance is simplified considerably, especially because direct measurements of pressure are rendered unnecessary. With an assumption of statistically independent wave and turbulent motions, the stresses due to the interaction of wave and turbulent velocities is neglected. In the surf zone, however, the breaking waves act as a turbulence production mechanism, and thus the wave and turbulent fluctuations may exhibit some degree of correlation. The resulting stresses are neglected, nevertheless, upon recognition that the turbulent motions are an order of magnitude smaller than the wave motion [Cox *et al.*, 1995], and do not contribute to the momentum balance in any substantive way. After depth-averaging and time-averaging along with the application of boundary conditions, the longshore momentum equation is expressed as

$$\overline{\rho \frac{\partial}{\partial x} \int_{z_b}^{\eta} uv dz} = \overline{\rho \frac{\partial}{\partial x} \int_{z_b}^{\eta} \tau_{xy} dz} - \overline{\tau_{by}}, \quad (1)$$

where  $\rho$  is the density of water,  $x$  is the cross-shore coordinate defined positive offshore,  $z$  is the vertical coordinate with  $z = 0$  at the still water level and  $z_b$  is the bottom position,  $\eta$  is the instantaneous free surface position,  $u$  and  $v$  represent the combined wave and current velocities in the cross-shore and longshore direction, respectively,  $\tau_{xy}$  represents the turbulent momentum flux, and  $\tau_{by}$  is the bottom shear stress. The overline indicates a time-averaging procedure where the interval of averaging is hundreds of wave periods for this study involving irregular waves.

[5] The first term in (1) represents the total forcing mechanism for the longshore current due to the organized oscillatory wave motion, the interaction of the steady currents, and a roller contribution. The relative importance of the latter two remains a topic of considerable interest. While it is common to neglect the steady contribution of the combined velocities,  $u$  and  $v$ , Svendsen and Putrevu [1994] concluded that the dispersive effects due to vertical non-uniformities was an order of magnitude larger than the turbulent mixing. Conversely, Kobayashi *et al.* [1997]

concluded that the dispersion effects due to the local nonuniformities may play a significant role for monochromatic waves, but proved unimportant for irregular waves. The inclusion of a roller contribution in the momentum balance by Ruessink *et al.* [2001] and others was shown to improve the cross-shore distribution of the longshore current on barred beaches.

[6] A great deal of effort has gone into the exploration of bottom shear stress models [e.g., Grant and Madsen, 1979] as the primary impedance force in the alongshore momentum balance. Without a description of the near-bed turbulence, the bottom shear stress is expressed with a quadratic drag law

$$\overline{\tau_{by}} = \rho c_f v \sqrt{u^2 + v^2}, \quad (2)$$

where  $c_f$  is a drag coefficient. This formulation for stress is an empirical result based on steady flow, but is, nevertheless, commonly applied in the surf zone. Several studies have indicated the suitability of the quadratic model in the nearshore region, but the examination of the alongshore oriented shear stress has been limited to field studies. Feddersen *et al.* [1998] showed a correlation between the combined wind and wave forcing and the bottom friction based on a quadratic friction formulation. Trowbridge and Elgar [2001] concluded that the quadratic drag law was accurate for energetic conditions by comparisons with the measured near-bottom turbulent Reynolds shear stress. At a smaller timescale, the time-dependent shear stress determined from measurements in a flume and presented by Cox *et al.* [1996] was faithfully described by the quadratic law.

### 3. Experimental Setup

[7] A brief description of the Large-Scale Sediment Transport Facility (LSTF) (Figure 1) is given herein, and the interested reader is referred to the exhaustive report on the design, instrumentation, and capabilities of the tank by Hamilton *et al.* [2000].

[8] The LSTF measures approximately 25 m in the cross-shore by 30 m alongshore where the walls are angled

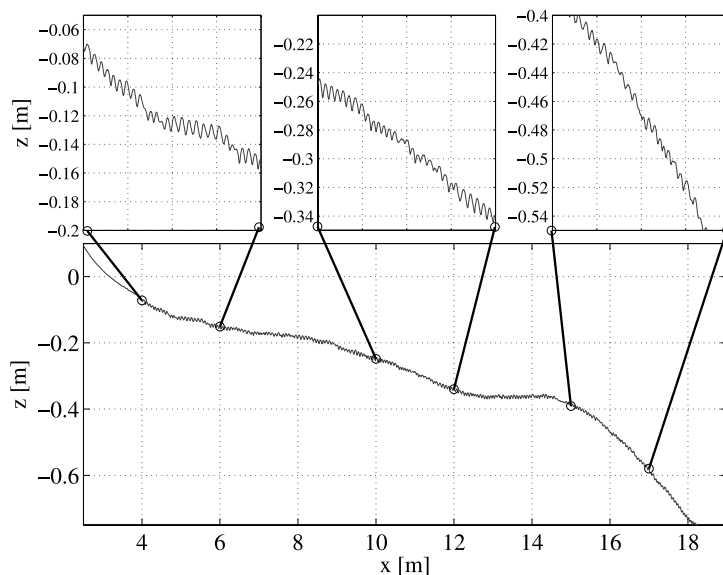


**Figure 2.** Bottom profile and detail of vortex ripples at  $y = 22$  m.

relative to a cross-shore transect to act as wave guides and minimize interference with the propagation of obliquely incident waves. Unidirectional waves were generated at a depth of 0.9 m in the LSTF with four synchronized paddles rotated to create long crests oriented  $10^\circ$  from the long straight shoreline. A pump system was designed to recirculate the wave-generated longshore current from the downstream boundary to the upstream boundary of the facility, thus allowing the laboratory basin to function as an infinitely long cylindrical coast. The cross-shore distribution of the longshore current is regulated by 20 independently controlled pumps through 20 channels at the downdrift end of the tank. Determining the proper pump rate was an iterative procedure, and the procedure details are given by *Hamilton and Ebersole* [2001].

[9] The sand beach was part of a larger sediment transport investigation, and comprises well-sorted quartz sand with a median grain diameter of 0.15 mm. Before the data collection began, the beach was exposed to wave action until a stable profile was realized, and the interested reader is referred to *Wang et al.* [2002] for details. The beach profiles were measured with a bottom-tracking profiler with a sampling rate sufficiently rapid to resolve the sand ripples. Figure 2 presents a measured profile near the center of the tank at  $y = 22$  m and smaller-scale detail plots showing the ripple geometry at three cross-shore locations. The bed stresses in a surf zone are typically large enough that ripples are washed out over a portion or all of the breaker region. Sand transport over the bar, in particular, is usually sheet flow transport. However, the flow conditions of the test detailed herein, were such that ripples were present over the majority of the surf zone, including the bar. It is likely that a slight increase in wave height would have produced a change in bed state. Indeed, the comprehensive study by *Tajima* [2004] of the LSTF bed state concludes that several models for ripple geometry classify a large portion of the surf zone as residing in the “break-off range,” meaning that a small increase in stress would result in a transition to sheet flow conditions. Ripples were statistically uniform along the beach, and with the exception of the swash zone, were

reasonably uniform in height and length across the beach. Just seaward of the swash zone, the ripples measured approximately 1 cm in height and 8 cm in length. The height and length of ripples in the midsurf zone measured 0.7 cm and 7 cm, similar in dimension to the ripples measured in the region immediately seaward of the bar with 0.6 cm and 7 cm. In combined wave and current environments, the ripple orientation can become irregular for sufficiently strong currents. In the portion of the tank that is used for this study, the ripple crests were visually observed to be wave-dominated, meaning that the crests were oriented essentially perpendicular to the wave propagation direction, from  $\sim 10^\circ$ – $5^\circ$  relative to a cross-shore transect. The coverage of bathymetric measurement is shown in Figure 3.

[10] Synchronized free surface elevation and velocities were collected from a movable instrument bridge spanning a cross-shore transect as shown in Figure 1. Ten capaci-

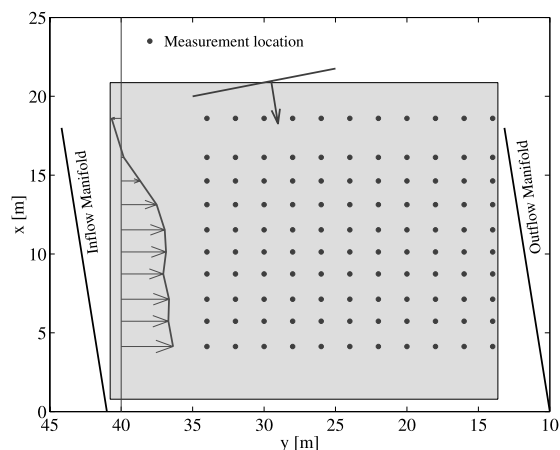


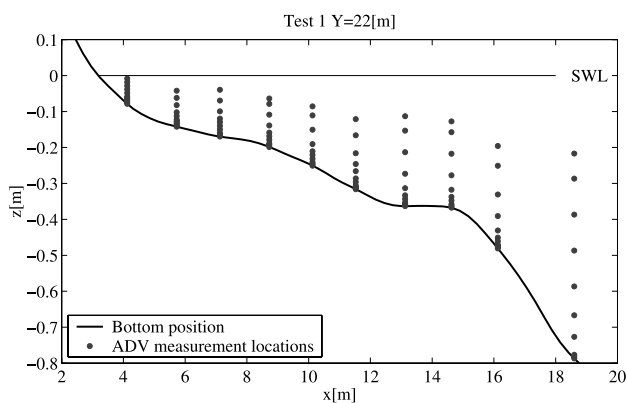
**Figure 3.** Plan view of the LSTF, where the shaded region shows the coverage of the bathymetry measurement, and the positions of the measurement locations for the horizontal coverage are depicted (circles).

**Table 1.** Cross-Shore Positioning of Instruments

ADV and Wave Gauge Number	Cross-Shore Position, m
1	4.125
2	5.725
3	7.125
4	8.725
5	10.125
6	11.525
7	13.125
8	14.625
9	16.125
10	18.600

tance-type surface piercing wave gauges, sampled at 20 Hz, were used to collect the free surface elevation. Velocity data were collected with acoustic doppler velocimeters (ADV) at the same position in the cross-shore and were synchronized with the wave gauge signals. The cross-shore position of the instruments is given in Table 1. Each sampling duration was ten minutes long, and complete horizontal and vertical coverage was accomplished by moving either the bridge or the instrument elevation. Stationarity in the wave field was assured by using the same wave paddle-position time series for each sampling duration, and the data were collected in two stages. The first stage focused on broad horizontal coverage where velocity measurements were taken at one third of the water depth from the bottom, and the horizontal measurement locations are shown on Figure 3. Detailed velocity data at ten positions over the vertical column were compiled during the second stage of each test for a single cross-shore transect at  $y = 22$  m. The vertical positioning of the measurement locations is shown in Figure 4.

[11] Irregular waves with TMA [Bouws *et al.*, 1985] spectral shape were generated with a peak period of  $T_p = 1.5$  s and a spectral peakedness parameter  $\gamma = 3.3$ . A piston-type wave paddle was used to generate waves in 90 cm of water, and the spectra of the free surface elevation, measured seaward of the breaking region at wave gauge 10, is shown in Figure 5. The measured spectral peak period is essentially equivalent to the specified period of  $T_p = 1.5$  s, and the specified value is used in this analysis. On the basis of the data at wave gauge 10, seaward of the breaking region, the root mean squared wave height measured

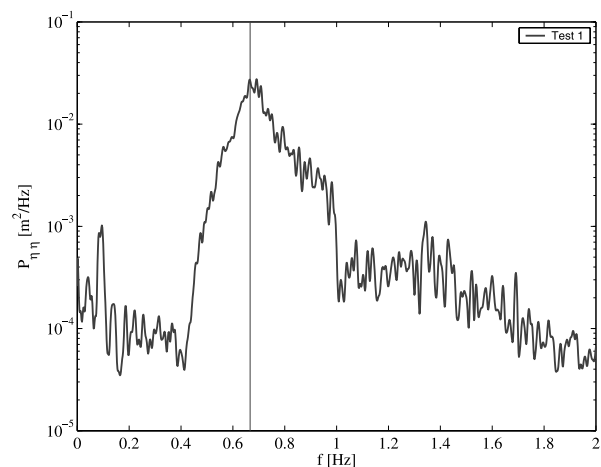
**Figure 4.** Measurement locations for vertical coverage phase (circles).

0.185 m, where  $H_{\text{rms}}$  is the high-pass filtered wave height. Spectral analysis of the variation in free surface position indicates significant low-frequency energy in the inner surf zone that is consistent with standing waves due to resonance in the closed basin. While the tank resonance has a pronounced effect on the free surface position variation near the shoreline, the waves do not break and do not contribute to the radiation stress in a manner well characterized by the spectral peak period and angle of propagation. It is thus argued that the most meaningful representation of wave height for this study of momentum flux does not include the low-frequency components. The wave height is computed as  $H_{\text{rms}} = \sqrt{8m_o(f > 1/3 \text{ s})}$  where  $m_o(f > 1/3 \text{ s})$  is the zero moment of the variance spectrum including only frequencies larger than half of the peak frequency and remains consistent with the analysis of Wang *et al.* [2002]. The irregular waves are classified as spilling breakers with a surf similarity parameter  $\xi = 0.15$  based on  $H_{\text{rms}}$ .

#### 4. Results

[12] The cross-shore distribution of wave heights is shown in Figure 6. Note that an analysis including the full spectrum of frequencies results in increased  $H_{\text{rms}}$  near the shoreline. Owing to the large number of transects, data from only half of the alongshore measurement positions are shown ( $y = 16, 20, 24, 28,$  and  $32$  m), and a measure of the longshore uniformity in wave heights can be judged from the degree of scatter in the alongshore direction.

[13] Time-averaged longshore velocities at the same transects are shown in Figure 7 where current magnitudes are measured at one third of the water depth from the bottom. With exception of the most shoreward and most seaward measurement locations, the standard deviation of the velocities measured between transects was less than 1 cm/s. The cross-shore distribution of longshore current velocity showed a sharp increase in velocity within the breaker region. The region extending from the outer surf zone to the still water shoreline is characterized by a broad, nearly uniform velocity profile with the highest measured velocities occurring in the most shallow region. Currents within the swash zone shoreward of ADV1 were not

**Figure 5.** Power spectral density of the free surface seaward of the breaker region, at measurement location 10.

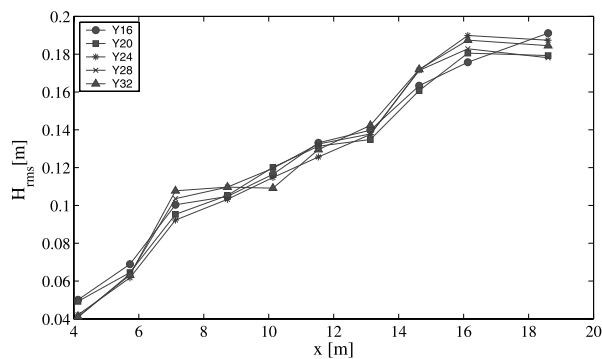


**Figure 6.** Cross-shore distribution of wave height at transects  $y = 16, 20, 24, 28,$  and  $32$  m.

systematically measured during these tests. Visual observations of injected dye, however, support measurements indicating large alongshore velocities near the shoreline. The longshore current direction at the most seaward gauge 10 reverses direction (Figure 7). This recirculation current is the undesirable artifact of the finite length of the basin, and may have influenced the distribution of the current, particularly in the outer surf zone.

#### 4.1. Contributions to Momentum Flux

[14] The detailed measurements taken of the internal velocity field during the vertical coverage phase of the tests are suitable for quantifying the terms of the alongshore momentum balance (1).

[15] As the waves shoal and break in the LSTF, coherent vortices are created and ultimately degenerate into turbulent fluctuations. These turbulent motions dominate surf zone characteristics such as the depth distribution of currents (Y. Tajima and O. S. Madsen, Surf zone hydrodynamics, submitted to *Journal of Waterway, Port, Coastal, and Ocean Engineering*, 2004, hereinafter referred to as Tajima and Madsen, submitted manuscript, 2004). The use of the data and a depth-integrated equation, however, reduces the need for an accurate description of the turbulence levels. Apart from the breaking wave decay and associated radiation stress gradients, the effect of turbulence is represented in the turbulent shear stress  $\tau_{xy}$ . The bottom shear stress  $\tau_{by}$  can also be expressed explicitly in terms of a near-bed Reynolds stress, but the alternative quadratic drag formulation is used herein. The turbulent shear stress acts as a mechanism to transfer momentum laterally, and is typically modeled with an eddy viscosity formulation [e.g., *Longuet-Higgins*, 1970a, 1970b] dependent on the cross-shore current rate of shear. While the analytical solution of *Longuet-Higgins* [1970a, 1970b] required the lateral mixing term to predict physically realistic longshore current velocity distributions for periodic waves, subsequent studies have demonstrated little effect of including this term for irregular waves. For instance, *Thornton and Guza* [1986] concluded that the lateral mixing was not needed to match measured field data of currents and irregular waves. *Stive and Wind* [1982] showed that the contribution of the turbulent momentum flux is small ( $\sim 5\%$ ) relative to the wave-induced momentum flux, and *Feddersen et al.* [1998] found that the turbulent momentum flux was small relative to the bottom shear stress. Given the former cited evidence of a

small contribution, coupled with the difficulties in estimating Reynolds stresses from ADV measurements, the effect of lateral mixing is neglected hereafter.

[16] The first term in (1) represents both a forcing mechanism due to the organized wave motion and the interaction of the steady currents. The decomposition of combined velocities into a steady ( $\bar{U}, \bar{V}$ ) and time-varying ( $\tilde{u}, \tilde{v}$ ) portion is straightforward at each velocity measurement location:

$$u = \bar{U} + \tilde{u}$$

$$v = \bar{V} + \tilde{v}.$$

However, significant momentum transfer occurs above the trough level, in a portion of the water column that is difficult to measure. *Stive and Wind* [1986] and others have imposed a shear stress at the trough level as a boundary condition and thus avoided a detailed analysis of the trough to crest region. The trough-level shear stress, however, was based on velocities according to linear theory as well as a roller model. Alternatively, a functional form for the velocities in the upper region is prescribed herein, and then used to quantify the momentum contribution. The upper region in this analysis is defined as the region extending from the highest measurement position ( $z_l$ ) to the instantaneous free surface position as shown in Figure 8. The prospect of integrating the time-dependent equations to determine the upper velocity field is clearly daunting, and an alternative approach is sought.

[17] The data analyzed by *Stive and Wind* [1982] were taken in a 2-D flume where velocities were measured with a laser doppler velocimeter. Measurements were not possible within the aerated portion of the breaking waves, and an extrapolated velocity field based on the depth integrated continuity equation was used. The alongshore uniformity of bathymetry and hydrodynamics in the LSTF can be exploited to enforce a vanishing time-averaged mass flux in the cross-shore direction. The form of the steady cross-shore velocity in the upper region is based on the measured steady velocity at  $z_l$  with a linear variation in the vertical, and the slope of the linear variation represents a free parameter set to satisfy the conservation of mass. The time-varying portion assumes narrow bandedness in fre-

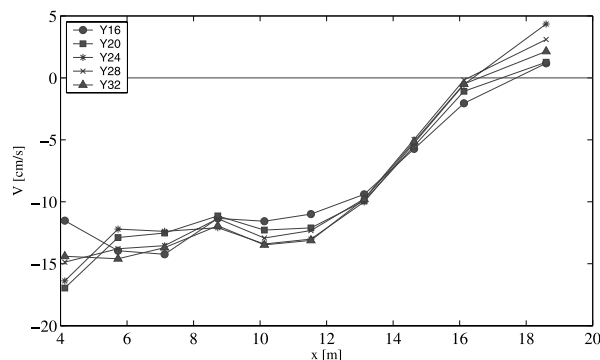


**Figure 7.** Cross-shore distribution of longshore current based on measurements at  $z = -2d/3$  for transects  $y = 16, 20, 24, 28,$  and  $32$  m.

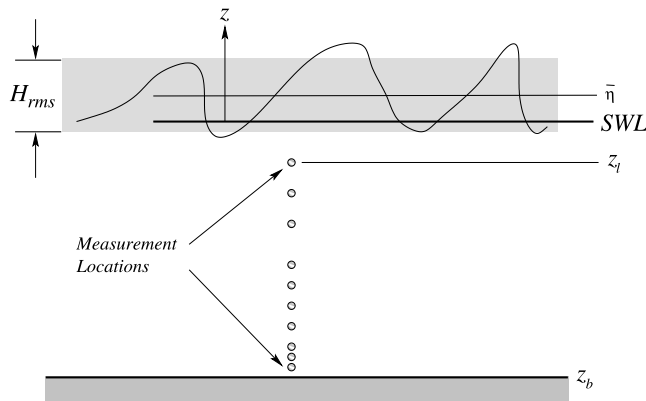


**Figure 8.** Definition sketch.

quency and is based on a measured oscillatory velocity  $\tilde{u}_{z_l}$  with a cosh dependence in  $z$ :

$$u_{up} = \overline{U}_{z_l} - C(z - z_l) + \tilde{u}_{z_l} \frac{\cosh k_p(h + z)}{\cosh k_p(h + z_l)}, \quad (3)$$

where  $k_p$  is the spectral peak wave number, and the time steady  $C$  is determined by the condition of zero cross-shore mass flux:

$$\int_{z_b}^{\eta} u \, dz = 0. \quad (4)$$

Through the nonzero specification of  $C$ , the cross-shore steady velocity profile given by (3) can exhibit a gradient at the trough level due to the exerted wave stress near the surface, consistent with the results of others [e.g., *Stive and Wind*, 1986]. Note that the synchronized velocity  $\tilde{u}_{z_l}$  and free surface elevation data allow for the representation of a shoreward mass flux in the trough to crest region. The contribution of mass flux from a roller is also included in a rudimentary way through the specification of the free parameter  $C$ . Tajima and Madsen (submitted manuscript, 2004) reiterate that the presence of a roller has a considerable effect on the magnitude of the return current, and, to a lesser extent, the roller contributes to the momentum balance. Rollers are understood to have little influence on the overall wave forcing in the surf zone, but change the spatial distribution. Imposing the correct total mass flux (through the free parameter) without the appropriate depth profile, however, provides no assurance that the momentum flux is represented accurately because momentum flux terms appear as the product of velocities and depend on the velocity distribution in  $z$ .

[18] To be consistent with linear theory, the horizontal time-varying velocities in the trough to crest region should be developed from a Taylor expansion about the mean free surface position. The cosh dependence in (3), however, is similar in shape to the first two terms of the Taylor expansion. Additionally, the actual vertical dependence for irregular waves may depend on frequency. These complexities coupled with the reality that the instantaneous profiles were not measured are the rationale for the use of the simple cosh dependence.

[19] In the absence of a wind stress, and for the small angles of wave incidence in the LSTF, the alongshore-oriented wave-induced stress near the surface is small, resulting in longshore current velocity profiles with insignificant slope at the trough level. Thus the mean current magnitude in the upper region are assumed to equal the steady current velocity measured at the highest vertical position:

$$v_{up} = \overline{V}_{z_l} + \tilde{u}_{z_l} \frac{\cosh k_p(h + z)}{\cosh k_p(h + z_l)} \tan(\alpha), \quad (5)$$

where  $\alpha$  is the incident wave angle relative to the beach normal for the peak frequency. The field data of *Garcez Faria et al.* [1998] demonstrated that the steady alongshore current velocities are well described by a logarithmic profile throughout most of the water column, and the data showed small gradients in the mean velocity just below the trough level. The measurements near the trough level in the LSTF also indicate that an assumption of zero vertical gradient for the steady longshore current velocities is suitable as shown in Figure 9. As a sensitivity check, the following analysis was conducted after assuming an alternative (log) profile for the steady current velocity, and no differences were discernible in the results. The time-varying alongshore velocity component in (5) was related trigonometrically to cross-shore velocity data to avoid likely errors in the direct measurements. Difficulties in directly measuring  $\tilde{v}$  include a relatively small oscillatory component relative to the steady current magnitude. Additionally, the small wave angles require accurate angular positioning of the instruments which is exceedingly difficult. Some of the issues plaguing the *Thornton and Guza* [1981] study such as directional spread and defining a longshore direction were avoided in the careful laboratory experiment; the issue of instrument alignment, however, proved problematic in both data sets. The small incident wave angle renders estimates of the alongshore component of the wave velocity extremely sensitive to the angular positioning of the ADV. For instance, at ADV 4, an alignment error of  $3^\circ$  would result in a misrepresentation of the alongshore oscillatory velocities of 50%. Casting longshore wave velocities in terms of the cross-shore velocities effectively avoids this error, but the accuracy is dependent on the assumption of unidirectionality. The wave angle  $\alpha$  is computed using Snell's law based on the incident peak period. In deep water, all incident waves propagate in the direction of the wave paddle motion. The spectral components of different frequencies, however, refract at different rates and generate a directional distribution in the surf zone. The validity of using a single wave angle  $\alpha$  in representing all irregular waves is dependent on the degree of directional spread which remains small throughout the LSTF. For instance, at measurement location 5, near the center of the tank, the tight directional band of  $\alpha \pm 1^\circ$  contained 65% of the variance. Frequencies below the band should undergo a greater measure of refraction, while higher-frequency energy is less affected. Frequency decomposition might allow for a variable wave angle, but such a treatment would be impractical for this study because synchronized velocities and free surface position measurements are used together in the analysis. An analysis limited to the region under the trough level including angular

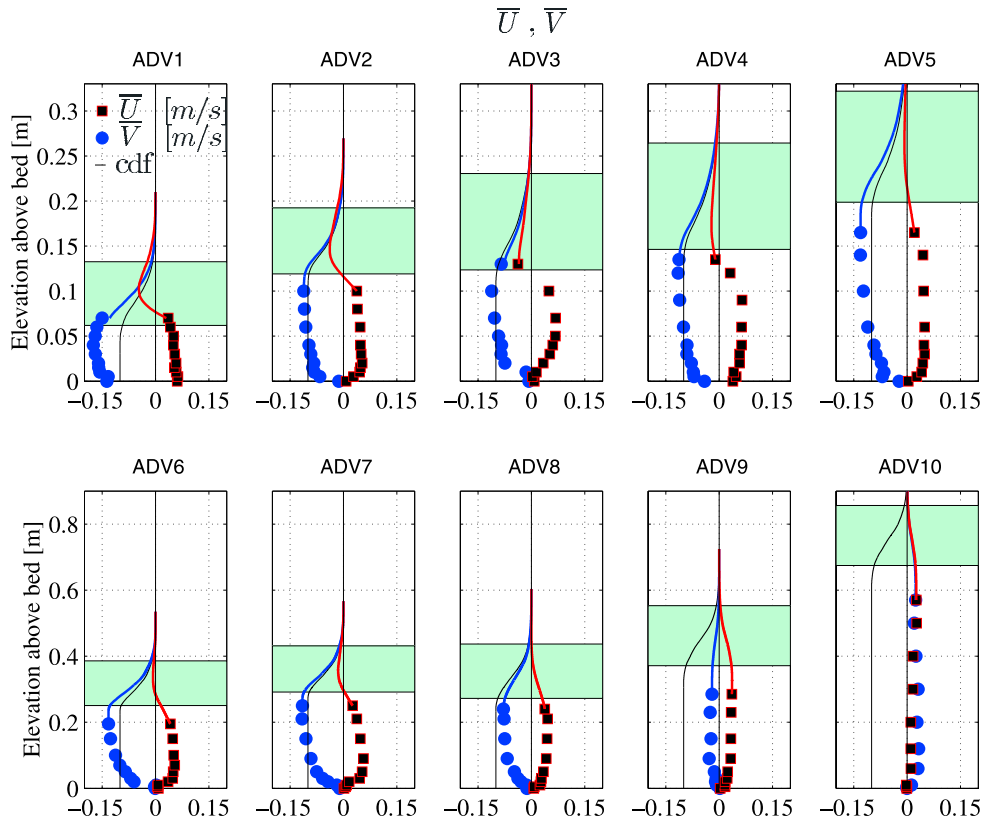


**Figure 9.** Steady horizontal velocities, where cross-shore velocities are shown as squares, longshore velocities as circles, and cumulative probability density function of the free surface as a solid line.

spread indicates that the error associated with the assumption of unidirectionality is only several percent of the wave-induced momentum flux.

[20] Figure 9 shows the depth variation of the steady current velocities at the ten cross-shore measurement locations. Data are shown as discrete symbols, and the prescribed steady velocities in the upper region are solid lines. The shaded region on each plot depicts the range of the root-mean-square wave height  $H_{\text{rms}}$  centered about the measured mean water level. Compared with the incident wave-induced velocities, the measured current velocities are less susceptible to errors introduced with imperfectly oriented instruments. The same alignment error of  $3^\circ$  discussed above results in errors of less than 1% in the longshore current velocity. Note that the depth integration of the measured and prescribed steady cross-shore current velocities do not result in a zero total mass flux; the balance is restored when the shoreward mass flux due to the waves is taken into account. The measured longshore current velocities are nearly depth uniform near the measurement level  $z_l$ , while the cross-shore current velocities show a significant slope toward the shore. These data at the highest measurement positions lend strength to the assumed current velocity profiles in the upper region in (3) and (5). The alongshore and cross-shore current velocities only have a momentum contribution at a vertical position  $z$  during the times  $\eta > z$ ; accordingly, steady velocities shown in Figure 9 are reduced for a measured cumulative probability distribution function (cdf) of the free surface elevation that is than unity.

[21] The standard deviations of the horizontal velocities are shown in Figure 10, where, as justified previously, the alongshore component is related to the cross-shore velocity. Measurements are indicated with discrete symbols, and the computed values in the upper region are shown as solid lines. One indicator of the appropriateness of the simple cosh dependence is the continuation from the measured to the computed values without excessive changes in slope, and Figure 10 shows that the transitions at  $z = z_l$  are realistic. At the offshore locations (ADV6–ADV10), below the strong modification by the cdf, there is an increase in the magnitude of the wave motions in the upper region compared with the measurements at  $z_l$ . This behavior is a result of the cosh dependence with depth and a cdf of unity near  $z = z_l$ . When compared with the steady current velocity profiles of Figure 9, the measurements taken near the bottom reveal that the effect of the boundary is confined to a relatively thin layer near the bed. The large near bottom gradient in the magnitude of oscillatory velocity when compared with steady current velocities is consistent with the extensive literature pertaining to wave and current boundary layers [e.g., *Grant and Madsen, 1979*]. Outside of the thin boundary layer but near the bottom, the velocities have little variation with depth, in accordance with the cosh dependence of linear waves. For comparison, an estimate of the cross-shore orbital velocities is developed from a spectral decomposition of  $\eta$  along with the linear relationship between free surface elevation and velocity for each component. When compared with the measurements, the linear representation is expectedly different within the thin

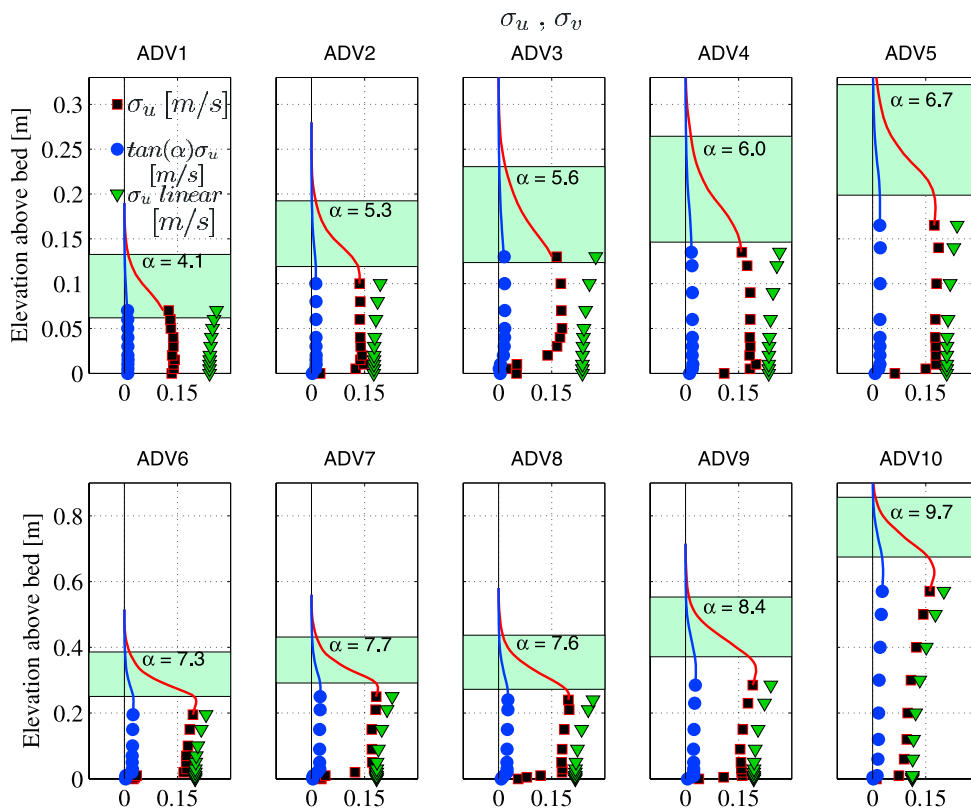


**Figure 10.** Standard deviation of the time-varying velocities, where cross-shore velocities are shown as squares and longshore velocities as circles.

wave boundary layer near the bed as linear theory is based on inviscid flow. The amplitude of the oscillatory motion is, however, overpredicted by the linear theory throughout the entire water column, even in the region above the boundary layer where the effect of the bed shear stress is minimal. *Guza and Thornton* [1980] also found that the velocity representation based on a measured free surface position was overpredicted, but to a lesser extent. The inner surf zone, however, demonstrates the greatest difference in the present data set, and the *Guza and Thornton* [1980] study did not extend into depths less than 1 m. The poor comparison results in an overprediction of the momentum flux due to the incident waves when using a linear representation of the radiation stress, as will be shown subsequently.

[22] The oscillatory and steady velocities previously presented can be used to develop the depth-dependent momentum fluxes. The depth distribution of the steady and time-varying contributions are shown in Figure 11, where the decomposition below the trough level is straightforward. At vertical positions that are intermittently above the free surface elevation, however, product terms comprise a steady and oscillatory component, in general, have a nonzero time average. These terms owe existence to both the time mean and time-varying velocities, and are thus not neatly apportioned to either contribution. In Figure 11, the cross terms are included with the steady contribution in order to remain consistent with the accepted definition for radiation stress as due to the wave components exclusively [e.g., *Mei*, 1989]. This distinction is largely academic, however, as the final momentum balance includes the terms

without differentiation. Because  $\bar{V}$  is fairly constant with depth, the steady product  $\bar{U} \bar{V}$  is similar in shape to the steady cross-shore velocity. The seaward oriented return flow results in a negative contribution in the lower region that is counteracted, in large part, by the presence of the shoreward directed mass flux near the surface. The wave component, in contrast, is directed onshore over the complete water column and is largest near the surface, but below the strong modification by the cdf. The combined time-varying and steady effects are also shown in Figure 11. Seaward of the surf zone, the combined  $\overline{uv}$  is dominated in shape and magnitude by the oscillatory velocities; As the waves break and lose energy throughout the surf zone, the shape is then dominated by the steady contribution. The total depth-integrated effect of  $\bar{U} \bar{V}$ , however, remains small.

#### 4.2. Bottom Shear Stress

[23] When neglecting the turbulent momentum flux in (1), the bottom shear stress is left as the sole balance for the cross-shore gradient in momentum flux. Values of shear stress can be computed with (2) using measured values and time-averaging over the total time series. Such estimates of  $\tau_{by}$ , however, are dependent on the vertical position used for collection of the total velocities  $u$  and  $v$ . The distance from the bed should be small relative to the water depth, but also well above the local influence of bed forms. To demonstrate the depth dependence of the shear stress divided by the drag coefficient  $\tau_{by}/c_f = \rho v \sqrt{u^2 + v^2}$ , the total measured velocities at each vertical location are used to develop an estimate of the shear stress as shown in Figure 12. For a given

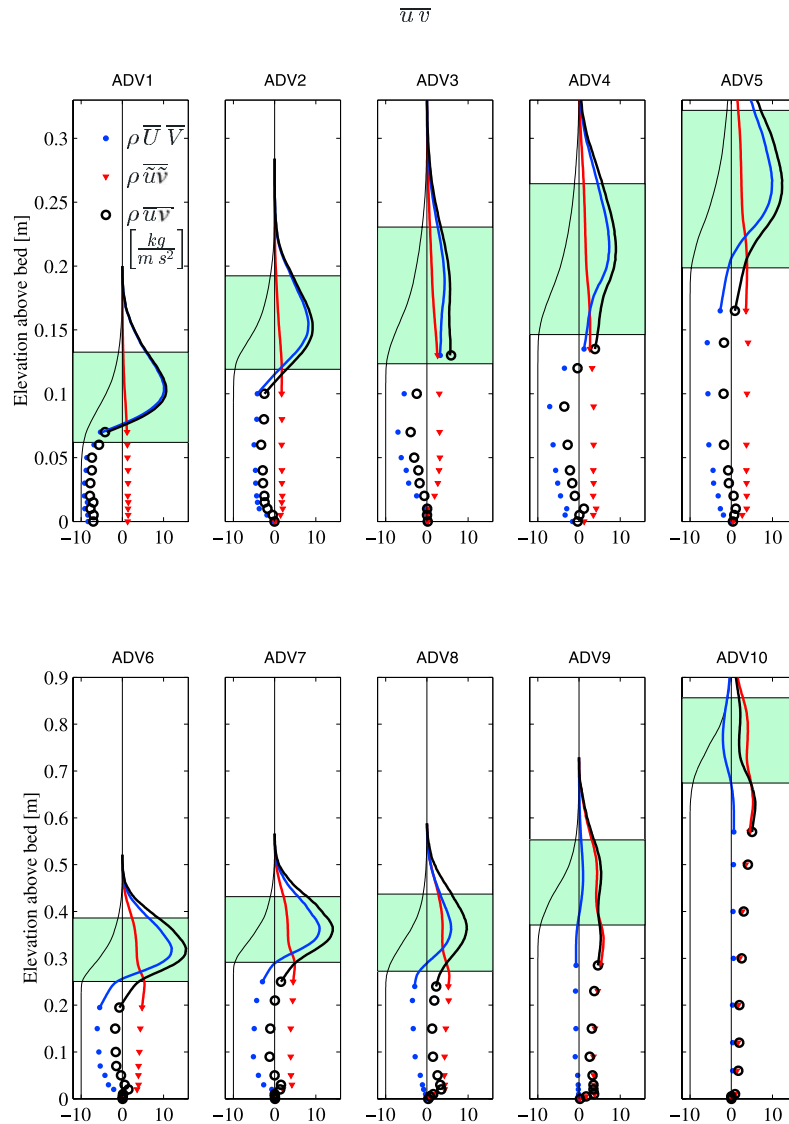


**Figure 11.** Vertical distribution of momentum flux, where steady contributions are shown as circles, time-varying contributions are shown as red inverted triangles, the combined total forcing is shown as open circles, and cumulative probability density function of the free surface is shown as a solid line.

constant drag coefficient, the computed shear stress was 10–15% larger using velocities at the midpoint of the still water depth when compared to the stress from a location one third of the depth from the bottom. *Garcez Faria et al.* [1998] avoided this ambiguity by using the magnitude of the velocities at the typical location for field studies of 1 m above the bed, and the depth-averaged  $\overline{V}$  thus reducing the depth dependence.

[24] Small-scale vortex ripples have a primary effect on the rate at which momentum is shifted from the fluid to the bed. Ripples such as seen in Figure 2 act to increase the shear stress for a given free-stream wave and current velocity. Alternatively, for a given shear stress, the presence of ripples acts to reduce the magnitude of the current velocity. The friction factor is commonly considered to be an increasing function of the relative bed roughness  $r/A$  where  $r$  is physical roughness length scale, and  $A$  is orbital amplitude of the fluid motion above the boundary layer [e.g., *Nielsen*, 1992]. Significant variations in the relative

bed roughness across the surf zone leads to considerable variations in the empirical drag coefficient. An alternative explanation for variable  $c_f$  was given by *Church and Thornton* [1993] who suggested that the modifications of the vertical mixing due to the remotely generated turbulence increases the momentum coupling between the fluid and the bed, effectively increasing the drag coefficient. Thus variations in the turbulence intensity through the surf zone may lead to a nonconstant drag coefficient. As a first approximation, however, the shear stress can be developed from a spatially constant coefficient, and compared with the gradient in momentum flux. Alternatively, the drag coefficient  $c_f$  can be treated as the unknown, and the results are presented in the following section.

## 5. Alongshore Momentum Balance

[25] In accordance with the separation procedure previously explained, the depth-integrated steady momentum

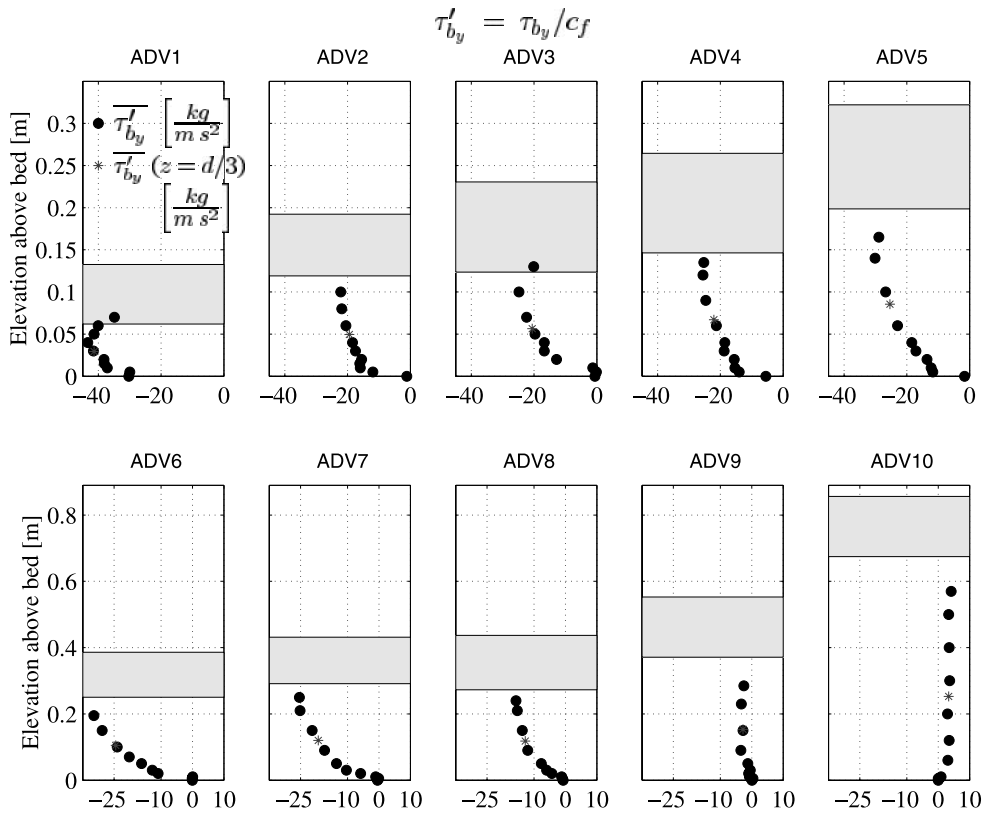


**Figure 12.** Bottom shear stress divided by  $c_f$  computed from measured velocities over the water column shown as circles and interpolated to a position  $z = -2d/3$  (asterisks).

flux and the flux due to the time-varying components are shown in the top panel of Figure 13. The cross-shore gradients of these total momentum fluxes are required subsequently, and small measurement errors or inaccuracies in the assumed velocity forms will act to create erratic numerical derivatives. *Feddersen et al.* [1998, 2003] and *Whitford and Thornton* [1993], for instance, used the bulk radiation stress (integrated over the surf zone) along with assumptions about the shoreline boundary condition to avoid this issue. *Svendson and Putrevu* [1993] used splines to smooth data before numerical differentiation of the wave height and setup. The momentum flux is expected to be a continuous and smooth function across the surf zone for irregular waves, so the data are represented by a fourth-order least-squared polynomial for the purpose of developing gradients. On the basis of conservation of energy flux on a long straight coast, it is readily shown that radiation stress is conserved seaward of the breaker region. The slope of the approximating functions at the seaward boundary, therefore, were designated to be zero, which appears to be consistent with the data. The momentum flux due to the oscillatory motion is a monotonically decreasing function across the surf zone as the waves break and lose energy. The steady contribution, on the other hand, is small in magnitude throughout the domain, but exhibits a maximum near the middle of the surf zone; the effect of this is explained later.

[26] The total combined steady and time-varying momentum flux integrated over the water column is shown in the middle panel of Figure 13. It is common to neglect the steady contribution and to use the linear representation of

the time varying velocities, leading to the familiar expression for radiation stress

$$S_{xy} = \frac{1}{8} \rho g H_{\text{rms}}^2 \frac{c_g}{c} \cos \alpha_p \sin \alpha_p, \quad (6)$$

where  $c_g$  is the group speed,  $c$  is the phase speed, and  $\alpha_p$  is the angle of wave propagation, all based on the spectral peak. The wave height  $H_{\text{rms}}$  used in the computation of the radiation stress is spectrally high-pass filtered as described previously. The expression (6) is developed on the basis of constant form progressive waves of infinitesimal wave slope over a flat bottom. Clearly, conditions in the surf zone violate each of these assumptions and the application should give us pause, but it remains widely employed nevertheless. The linear representation of radiation stress at each measurement location is shown in the second panel along with the fourth-order least-squared polynomial.

[27] Over the entire domain, the linear radiation stress is substantially larger than the computed momentum flux. From the seaward boundary to the mid surf zone ( $x \sim 8$  m), for instance,  $S_{xy}(\text{linear})$  is approximately 50% larger than the measured representation. Further inshore ( $x < 8$  m) the difference is more prominent. If, alternatively, the full spectrum is used in the development of  $H_{\text{rms}}$ , the radiation stress is increased by approximately  $0.2 \text{ kg/s}^2$  over the entire surf zone. The difference is inconsequential over most of the surf zone, but increases the overestimation in the inner surf zone where the radiation stress is small. The previously mentioned approach used by *Feddersen et al.* [2003] and

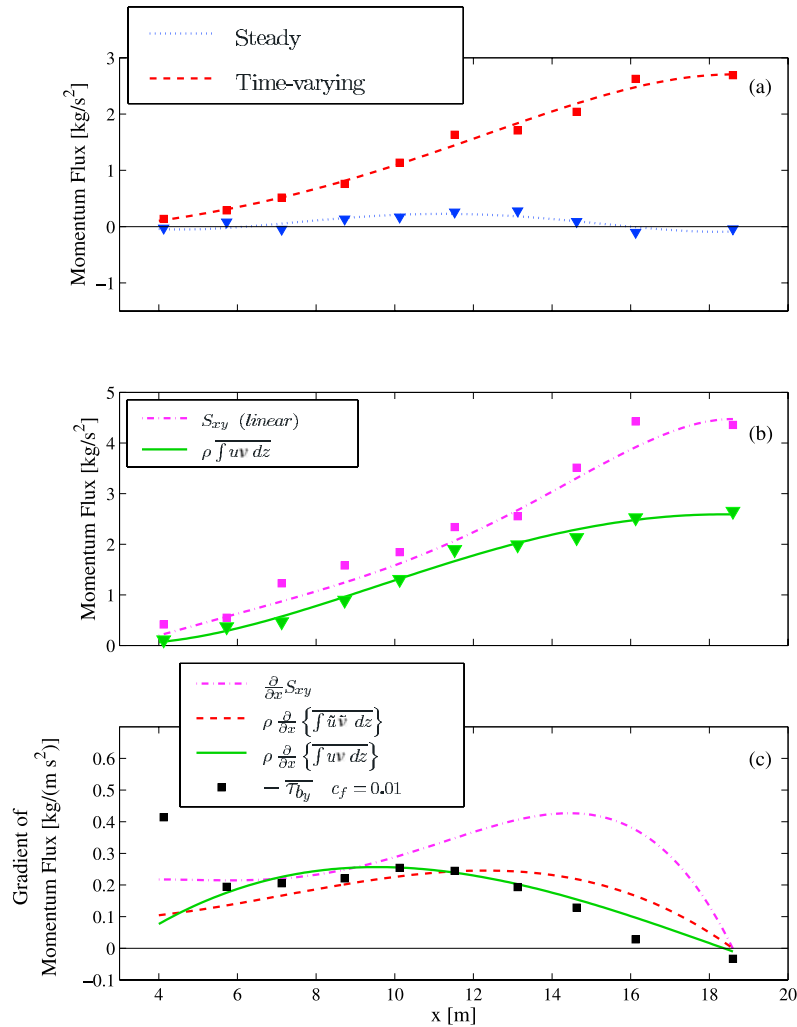


**Figure 13.** (a) Depth-integrated momentum flux from the steady and time-varying contributions. (b) Total measured momentum flux and the linear representation of radiation stress. (c) Cross-shore gradients of the linear radiation stress, time-varying contribution to the momentum flux, and total measured momentum flux. Also, the bottom shear stress computed with a spatially uniform  $c_f$  is shown.

others (integrating the momentum equation over the surf zone) would be based on only the data at the seaward most measurement location, which would lead to the conclusion that the linear radiation stress was approximately 65% larger than the measured representation. Recently, *Svendsen et al.* [2003] reported on the cross-shore momentum equation and the reasonably good representation of setup due to the gradient in the linear radiation stress. While radiation stress is indeed overrepresented, the linear theory underprediction of wave height acts, to some degree, to cancel this inaccuracy. It is implied, therefore, that the use of a measured wave height would lead to a value for linear theory-based radiation stress that was too large and an overprediction of the setup. In a practical sense, *Svendsen et al.* [2003] suggest that the use of Sine wave theory in modeling wave height and representing radiation stress gives reasonable results due to these two counteracting errors. Alternative representations of the wave hydrodynamics in the surf zone may be more satisfactory in determination of bulk parameters. *Hansen* [1990], for instance, used laboratory data to

develop empirical expressions for the radiation stress within the surf zone. The data, however, were limited to periodic wave cases, and the applicability to irregular waves is uncertain and is not included herein.

[28] The analysis of *Trowbridge and Elgar* [2001] included a study of the local alongshore momentum balance. The forcing accounted for wind stress and a gradient in the linear representation of radiation stress. The bottom shear stress was not based on a quadratic friction formulation, but was directly measured from the turbulent vertical flux of horizontal momentum near the bed  $\overline{\tau}_{by} = -\rho \overline{v'w'}$ . This approach has the advantage of stress estimates without reliance on empiricism. When the forcing and bottom stress terms were compared, the forcing was a factor of two larger in size. The wind shear was included in the balance, but was considered unlikely to cause the discrepancy due to the relatively small magnitude when compared to the wave stress. The authors concluded that the difference in forcing and friction was possibly due to a linear wave stress estimate that was too large. Many other alongshore mo-

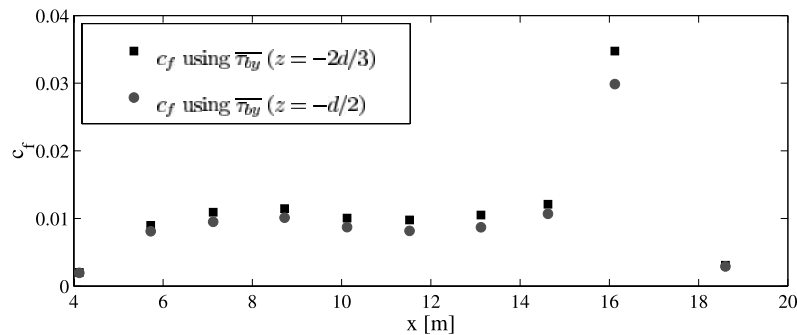


**Figure 14.** Cross-shore distribution of computed drag coefficients using measured velocities at  $z = -2d/3$  shown as squares and using measured velocities at  $z = -d/2$  (circles).

mentum balance studies use the quadratic drag law and calibrated coefficient, and any misrepresentations of wave forcing may be absorbed into  $c_f$ .

[29] The bottom panel of Figure 13 depicts three representations of the gradient in momentum flux as well as an estimate of the bottom shear stress based on a constant coefficient. Gradients are developed from the polynomial fit to the data explained previously, and it should be noted that the three versions of forcing are sensitive to the order of the polynomial fit and the zero slope imposed at the offshore boundary.

[30] The bottom shear stress was based on the time series of velocities measured at a distance of one-third of the depth from the bottom, which was the location found to have a steady current velocity that closely approximates the depth-averaged current velocity [Hamilton and Ebersole, 2001]. The empirical drag coefficient of  $c_f = 0.01$  was determined to match the gradient of measured momentum flux well, but is somewhat larger than values determined in field studies. A discussion of this difference follows.

[31] The total forcing based on measurements is considered to be an accurate representation which accounts for time-varying, steady, and wave roller contributions. The bottom panel of Figure 13 shows good agreement between the total forcing and the simple bottom shear stress with a spatially uniform drag coefficient. As shown previously, the time-varying forcing is dominant, and the other components have a smaller contribution. When the time-varied part is considered alone, the peak of the forcing occurs seaward of the peak of the total forcing, and does not balance the cross-shore variation of the estimated shear stress as skillfully. The better comparisons with the total forcing may be the consequence of implicitly including the roller contribution, where the roller functions to sink momentum in the outer zone and to release it closer to the shoreline. The gradient of the linear radiation stress is markedly different in magnitude and shape when compared to the measured forcing. A distinct peak is seen in the outer surf zone followed by a region of relatively low forcing in the inner zone and an increase in the very shallow water near the shoreline. Again, the increase in forcing at the shoreline based on  $H_{rms}$  may be due to the low-frequency resonance energy that is substantial near the shoreline. Overall, the linear forcing is not well balanced by the bottom shear stress estimates with a constant drag coefficient.

[32] The data from an additional test case (the Plunging Test Case of Wang *et al.* [2002]) was analyzed using the

procedure described above. Waves with a spectral peak period of 3 s and offshore  $H_{rms} = 19.4$  cm developed into mostly plunging breakers and generated peak longshore current velocities of approximately 17 cm/s. Under these energetic conditions, several instrumentation issues and bed position changes confounded the effort to get a complete data set as presented and used in the above analysis. While data for time-averaged quantities are reliable, only six of the ten cross-shore measurement locations yielded synchronized data valuable in developing momentum fluxes. The sparse data is, therefore, not presented here. The results of the analysis, however, supported the results presented above. The gradient in linear wave radiation stress was approximately twice as large as the measured forcing. Additionally, the peak of measured forcing was well inshore the peak linear wave forcing.

[33] The cross-shore variation in the drag coefficient  $c_f$  can be determined using measured velocities and assuming a match of the bottom shear stress and total measured forcing, combining (1) and (2). Figure 14 shows the cross-shore distribution of the drag coefficient using measured velocities. To demonstrate the degree of depth dependence of the computed coefficients, the balance is enforced using velocities measured at locations  $z = -2d/3$  and  $z = -d/2$ . Owing to the larger velocities at the middepth, the computed coefficients are smaller by 5–15% at most measurement locations. Across most of the surf zone,  $c_f$  was fairly uniform with a value of approximately 0.01; one exception is at measurement location 9 ( $x = 16.125$  m), where the steady longshore current velocity is nearly zero, and results should not be considered reliable. Also, near the shoreline, the absence of bed forms may contribute to the smaller  $c_f$ , and the use of a spatially uniform coefficient may be inappropriate there. The use of a coefficient that is artificially large in this location would account for the disparity between the gradient of momentum flux and the bottom shear estimate given previously. The computed drag coefficients over most of the domain are consistent with earlier studies (Longuet-Higgins [1970a, 1970b] used  $c_f = 0.01$  in the surf zone), but are somewhat larger than in recent field studies [Feddersen *et al.*, 2003; Garcez Faria *et al.*, 1998]. This difference may be due to the small water depth of the laboratory experiment when compared to the field studies. Garcez Faria *et al.* [1998] demonstrated that the coefficient is an increasing function of the physical bottom roughness normalized by the mean water depth  $r/d$ , and examined friction in the range of  $r/d = 0.001$ – $0.04$ .

Extrapolation of the results to a value characteristic of this experiment  $r/d \sim 0.02$  would lead to values of  $c_f$  that are similar to those presented in Figure 14. The difference may also be due to breaking induced turbulence that more readily penetrates the water column and effects the near-bottom shear stress in shallow water. Nevertheless, no laboratory studies of friction coefficients with waves and currents oriented at large angles over movable beds with vortex ripples are available for comparison.

## 6. Summary and Conclusions

[34] An experiment was conducted in a large-scale wave basin with the intent to simulate an idealized longshore uniform coast. Pumps were used to match the longshore currents generated by the breaking of obliquely incident irregular waves. The beach was comprises well sorted sand with a median grain diameter of 0.15 mm, and the majority of the bed was covered with vortex ripples. The wave height and steady current velocity measured over 11 cross-shore transects demonstrate that longshore uniformity is attained, and the momentum balance is simplified accordingly. Data collected at a single transect with ten measurement locations over the water column are used to quantify the terms of the momentum balance. Recognizing that significant momentum flux occurs in the region above the trough level of the waves, a method of extrapolation for the region above the highest measurement location is presented. On the basis of measured velocities, conservation of cross-shore mass flux, and Snell's law, both the steady current velocities and time-varying velocities in the upper region are shown to smoothly transition from the measured region to the extrapolated region. The enforcement of a vanishing integrated mass flux in the cross-shore effectively imposes a volume flux due to a wave roller. The momentum flux, however, is only considered in a rudimentary way as the vertical distribution of the roller induced flux is not taken into account.

[35] With a measured and extrapolated velocity field, the depth distribution of momentum flux is determined. The time-varying momentum flux is positive over the water column, and the steady contribution mirrors the shape of the steady cross-shore current velocity profile, oriented in the direction of wave propagation near the surface and seaward below the trough level.

[36] The bed shear stress is considered to be the primary balance to the gradients in alongshore oriented momentum flux. A quadratic drag law formulation and measured velocity time series are used to estimate the time-averaged bottom shear stress, but the computation is dependent on the distance from the bed to the measurement location.

[37] The gradient of the total depth-integrated momentum flux is shown to agree well with a bed shear stress estimate using a spatially uniform drag coefficient. While the forcing is dominated in magnitude by the time-varying contribution, including the steady currents (and a roller contribution) has the effect of shifting the peak forcing shoreward and improves the agreement with the bottom shear stress. In keeping with a limited number of studies, the linear representation of wave-induced forcing is shown to be larger by a factor of two than the measured estimate, and has a different cross-shore distribution. Others have found that the wave forcing given by linear theory is well correlated with a

quadratic bottom shear stress, but an exaggerated forcing may have been absorbed into the unknown drag coefficient without effect on the degree of correlation.

[38] **Acknowledgments.** We acknowledge the Chief of Engineers, U.S. Army Corps of Engineers, for permission to publish this paper. Support for B.D.J. and J.M.S. was provided through the Advanced Nearshore Circulation work unit of the U.S. Army Corps of Engineers Navigation Systems Research Program.

## References

- Bouws, E., H. Gunther, W. Rosenthal, and C. L. Vincent (1985), Similarity of the wind wave spectrum in finite depth water: 1. Spectral form, *J. Geophys. Res.*, *90*, 975–986.
- Church, J. C., and E. B. Thornton (1993), Effects of breaking wave induced turbulence within a longshore current model, *Coastal Eng.*, *20*, 1–28.
- Cox, D. T., N. Kobayashi, and A. Okayasu (1995), Experimental and numerical modeling of surf zone hydrodynamics, *Res. Rep. CACR-95-07*, Cent. for Appl. Coastal Res. Univ. of Del., Newark.
- Cox, D. T., N. Kobayashi, and A. Okayasu (1996), Bottom shear stress in the surf zone, *J. Geophys. Res.*, *101*, 14,337–14,348.
- Feddersen, F., R. T. Guza, S. Elgar, and T. H. C. Herbers (1998), Along-shore momentum balances in the nearshore, *J. Geophys. Res.*, *103*, 15,667–15,676.
- Feddersen, F., E. Gallagher, R. T. Guza, and S. Elgar (2003), The drag coefficient, bottom roughness, and wave-breaking in the nearshore, *Coastal Eng.*, *48*, 189–195.
- Garcez Faria, A. F., E. B. Thornton, T. P. Stanton, C. V. Soares, and T. C. Lippmann (1998), Vertical profiles of longshore currents and related bed shear stress and bottom roughness, *J. Geophys. Res.*, *103*, 3217–3232.
- Grant, W. D., and O. S. Madsen (1979), Combined wave and current interaction with a rough bottom, *J. Geophys. Res.*, *84*, 1797–1808.
- Guza, R. T., and E. B. Thornton (1980), Local and shoaled comparisons of sea surface elevations, pressures, and velocities, *J. Geophys. Res.*, *85*, 1524–1530.
- Hamilton, D. G., and B. A. Ebersole (2001), Establishing uniform long-shore currents in a large-scale laboratory facility, *Coastal Eng.*, *42*, 199–218.
- Hamilton, D. G., B. A. Ebersole, E. R. Smith, and P. Wang (2000), Development of a large-scale laboratory facility for sediment transport research, *Tech. Rep. ERDC/CHL TR-01-22*, U.S. Army Eng. Waterw. Exper. Stat., Vicksburg, Miss.
- Hansen, J. B. (1990), Periodic waves in the surf zone: Analysis of experimental data, *Coastal Eng.*, *14*, 19–41.
- Kobayashi, N., E. A. Karjadi, and B. D. Johnson (1997), Dispersion effects on longshore currents in surf zones, *J. Waterw. Port Coastal Ocean Eng. ASCE*, *123*, 240–248.
- Longuet-Higgins, M. S. (1970a), Longshore currents generated by obliquely incident sea waves, 1, *J. Geophys. Res.*, *75*, 6778–6789.
- Longuet-Higgins, M. S. (1970b), Longshore currents generated by obliquely incident sea waves, 2, *J. Geophys. Res.*, *75*, 6790–6801.
- Mei, C. C. (1989), *The Applied Dynamics of Ocean Surface Waves*, World Sci., Hackensack, N. J.
- Nielsen, P. (1992), *Coastal Bottom Boundary Layers and Sediment Transport*, World Sci., Hackensack, N. J.
- Reniers, A. J. H. M., and J. A. Battjes (1997), A laboratory study of long-shore currents over barred and non-barred beaches, *Coastal Eng.*, *30*, 1–21.
- Ruessink, B. G., J. R. Miles, F. Feddersen, R. T. Guza, and S. Elgar (2001), Modeling the alongshore current on barred beaches, *J. Geophys. Res.*, *106*, 22,451–22,463.
- Soulsby, R. L. (1998), Coastal sediment transport: The COAST3D project, *Proc. 26th Coastal Eng. Conf. ASCE*, *3*, 2548–2558.
- Stive, M. J. F., and H. G. Wind (1982), A study of radiation stress and set-up in the nearshore region, *Coastal Eng.*, *6*, 1–25.
- Stive, M. J. F., and H. G. Wind (1986), Cross-shore mean flow in the surf zone, *Coastal Eng.*, *10*, 325–340.
- Svendsen, I. A., and U. Putrevu (1993), Surf zone wave parameters from experimental data, *Coastal Eng.*, *19*, 283–310.
- Svendsen, I. A., and U. Putrevu (1994), Nearshore mixing and dispersion, *Proc. R. Soc. London, Ser. A*, *445*, 561–576.
- Svendsen, I. A., W. Qin, and B. A. Ebersole (2003), Modelling waves and currents at the LSTF and other laboratory facilities, *Coastal Eng.*, *50*, 19–45.
- Tajima, Y. (2004), Waves, currents, and sediment transport in the surf zone along long, straight beaches, Ph.D. thesis, Mass. Inst. of Technol., Cambridge.

- Thornton, E. B., and R. T. Guza (1981), Longshore currents and bed shear stress, in *Proceedings Directional Wave Spectral Applications*, pp. 147–164, Am. Soc. of Civ. Eng., Reston, Va.
- Thornton, E. B., and R. T. Guza (1986), Surf zone longshore currents and random waves: Field data and models, *J. Phys. Oceanogr.*, *16*, 1165–1178.
- Trowbridge, J., and S. Elgar (2001), Measurements of surf zone turbulence, *J. Phys. Oceanogr.*, *31*, 2403–2417.
- Visser, P. J. (1984), Uniform longshore current measurements and calculations, *Proc. 19th Coastal Eng. Conf. ASCE*, *2*, 2192–2207.
- Wang, P., B. A. Ebersole, E. R. Smith, and B. D. Johnson (2002), Temporal and spatial variations of surf-zone currents and suspended sediment concentration, *Coastal Eng.*, *46*, 175–211.
- Whitford, D. J., and E. B. Thornton (1993), Comparison of wind and wave forcing of longshore currents, *Cont. Shelf Res.*, *13*, 1205–1218.

---

B. D. Johnson and J. M. Smith, Coastal and Hydraulics Laboratory, Engineering Research and Development Center, Vicksburg, MS 39180, USA. (bradley.d.johnson@erdc.usace.army.mil; jane.m.smith@erdc.usace.army.mil)